# Critical Frequency in Nuclear Chiral Rotation

P. Olbratowski,[1,2] J. Dobaczewski,[1,2] J. Dudek,[2] and W. Płóciennik[3]

[1]*Institute of Theoretical Physics, Warsaw University, Hoża 69, PL-00681 Warsaw, Poland*

[2]*Institut de Recherches Subatomiques, CNRS-IN2P3/Université Louis Pasteur, F-67037 Strasbourg Cedex 2, France*

[3]*The Andrzej Sołtan Institute for Nuclear Studies, PL-05400 Świerk, Poland*

(Received 12 March 2004; published 29 July 2004)

Self-consistent solutions for the so-called planar and chiral rotational bands in $^{132}$La are obtained for the first time within the Skyrme-Hartree-Fock cranking approach. It is suggested that the chiral rotation cannot exist below a certain critical frequency which under the approximations used is estimated as $\hbar\omega_{\rm crit} \approx 0.5$–$0.6$ MeV. However, the exact values of $\hbar\omega_{\rm crit}$ may vary, to an extent, depending on the microscopic model used, in particular, through the pairing correlations and/or calculated equilibrium deformations. The existence of the critical frequency is explained in terms of a simple classical model of two gyroscopes coupled to a triaxial rigid body.

DOI: 10.1103/PhysRevLett.93.052501 PACS numbers: 21.10.Re, 21.30.Fe, 21.60.Jz, 27.60.+j

Chirality is an important phenomenon on the subatomic scale, in particular, in nuclear structure physics. Yet, the mathematical realizations of the associated symmetry operator encountered in the literature sometimes differ. As discussed in [1], the $\hat{R}^T$ operator, the product of the time reversal and a rotation through 180°, provides a possible realization of this symmetry in nuclei. Since $\hat{R}^T$ is a dichotomic symmetry [$(\hat{R}^T)^2 = 1$], its spontaneous breaking leads to doublets of closely lying rotational bands. Recently, pairs of bands that may originate from the breaking of $\hat{R}^T$ symmetry have been found in the $A \approx 130$ nuclei [2]. It has been suggested in [3] that $\hat{R}^T$ symmetry may be violated in these nuclei if one proton occupies a low substate of an $h_{11/2}$ orbital, and one neutron hole is left in a high $h_{11/2}$ substate. The former drives the nucleus towards elongated shapes, while the latter towards oblate ones. The interplay of these opposite tendencies may result in a shape resembling a triaxial ellipsoid. In the triaxially deformed potential, the particle and hole prove to align their angular momenta along the short ($s$) and the long ($l$) axes, respectively. As expected from the hydrodynamical model of rotation [4], the moment of inertia with respect to the medium ($m$) axis is the largest, favoring the collective rotation around this axis. Thus, the total angular momentum vector has nonzero components on all the three axes. If those three component-vectors form, say, a left-handed set, then $\hat{R}^T$ will transform them into a right-handed one. The resulting set cannot be superposed with the original one by any rotation, and we say, according to Kelvin's definition, that the system manifests chirality.

The newly found doublet bands [2], were extensively studied within the particle-rotor model [5] that supported their possibly chiral character. These bands can also be examined within the microscopic cranking approach, in which the wave function of the rotating nucleus is approximated by the Slater-determinant solution to the single-particle (SP) Routhian

$$\hat{h}' = \hat{h} - \boldsymbol{\omega} \cdot \hat{\boldsymbol{I}}, \tag{1}$$

where $\boldsymbol{\omega} = \{\omega_x, \omega_y, \omega_z\}$ denotes three Lagrange multipliers (sometimes interpreted as rotational frequencies), $\hat{\boldsymbol{I}}$ is the angular momentum operator, and $\hat{h}$ represents the mean field Hamiltonian. The chirality can be accounted for within the three-dimensional tilted axis cranking (TAC) method [6], which allows for an arbitrary orientation of the angular momentum vector in the intrinsic frame. The TAC chiral solutions have already been obtained with phenomenological mean field [7]. The present work reports on the first application of the self-consistent Hartree-Fock (HF) method, in which the mean potential is generated entirely from an effective two-body interaction. Such an approach is based on a more fundamental formalism, provides a strong test of the chiral geometry, and includes important effects such as current polarizations.

Realistic Skyrme interactions, SLy4 [8] and SKM* [9] were used in the HF calculations. The parity was kept as a conserved symmetry, and the pairing correlations were not included. The calculations were done using the code HFODD (v2.05c) [10,11] working in the harmonic oscillator basis. Twelve spherical shells were taken; increasing this number up to 16 changes the quantities of importance (deformation, moments of inertia, alignments, etc.) by less than 1%. The present study focuses on the discussed $\pi h_{11/2}^{1} \nu h_{11/2}^{-1}$ configuration in $^{132}$La. In all HF solutions found, a stable triaxial deformation of $\beta \approx 0.25$ and $\gamma \approx 45°$ was obtained.

To study the rotational properties in question, it is instructive to examine how a valence $h_{11/2}$ proton particle and an $h_{11/2}$ neutron hole respond to rotation. This can be done by using the standard principal axis cranking (PAC). Cranking about the $i$th principal axis ($i = s, m, l$) with frequency $\omega_i$ gives the angular momentum alignment $j_i$ on this axis. The calculated SP alignments of the valence particle and hole are given in Fig. 1. At $\omega = 0$, the

 © 2004 The American Physical Society 

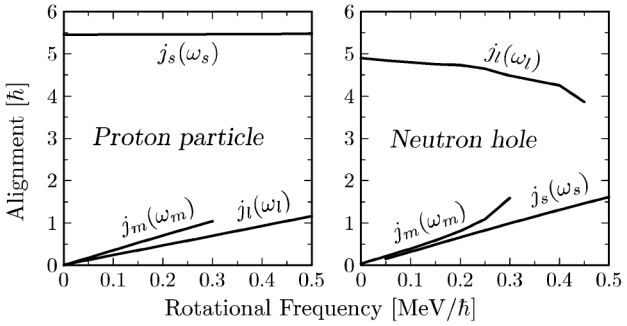


FIG. 1. Single-particle alignments of the valence $h_{11/2}$ proton particle and neutron hole, obtained from the HF PAC calculations with the SLy4 force, for cranking about the short, medium, and long axes.

particle and the hole do indeed orient their spins, $\boldsymbol{j}^p$ and $\boldsymbol{j}^h$, on the short and long axis, respectively. The response of $\boldsymbol{j}^p$ and $\boldsymbol{j}^h$ to rotation is rather weak, meaning that the SP wave functions are strongly constrained by deformation (deformation-alignment). These results can be summarized as

$$\boldsymbol{j}^p \simeq s_s \hat{\mathbf{1}}_s + \delta \mathcal{J}^p \boldsymbol{\omega}, \qquad \boldsymbol{j}^h \simeq s_l \hat{\mathbf{1}}_l + \delta \mathcal{J}^h \boldsymbol{\omega}, \tag{2}$$

where $\hat{\mathbf{1}}_s$ and $\hat{\mathbf{1}}_l$ are the unit vectors along the short and long axes, respectively. Therefore, to a reasonable approximation, the odd particle and hole can be treated like gyroscopes of spins $s_s$ and $s_l$, rigidly fixed along the short and long axes, while small coefficients $\delta \mathcal{J}^p$ and $\delta \mathcal{J}^h$, can be incorporated into the total inertia tensor $\mathcal{J}$.

The same PAC calculations provide the total alignments, $I_i$, that are plotted in Fig. 2. At zero frequency, cranking around the medium axis gives a vanishing angular momentum, while those around the other two axes give nonzero values equal to the SP alignments of the odd particle and hole, $s_s$ and $s_l$, respectively. The dependence of $I_i$ on $\omega_i$ is nearly linear, like for the rigid rotation, and the corresponding slopes give the microscopic collective moments of inertia associated with the principal axes, $\mathcal{J}_s$, $\mathcal{J}_m$, and $\mathcal{J}_l$. They already contain the contributions, $\delta \mathcal{J}^p$ and $\delta \mathcal{J}^h$ of Eq. (2).

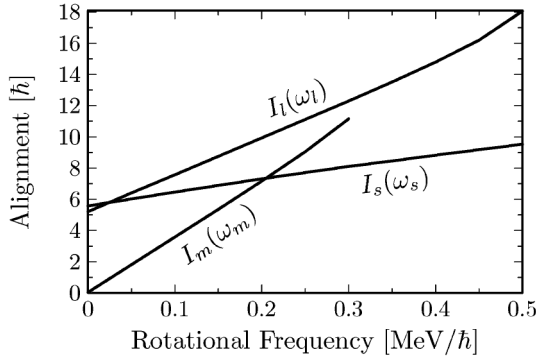


FIG. 2. Similar to Fig. 1, but for total alignments.

The microscopic PAC results presented so far suggest that the considered system can be modeled with the help of two gyroscopes of spins $s_s$ and $s_l$ rigidly fixed along the short and long axes of a triaxial rigid rotor characterized by the inertia tensor $\mathcal{J}$. We have checked within the HF TAC method that the off-diagonal components of $\mathcal{J}$ are negligibly small; in the model we set the diagonal components equal $\mathcal{J}_s$, $\mathcal{J}_m$, $\mathcal{J}_l$. It is instructive to solve the associated problem of the motion in a classical framework and show that it faithfully represents salient features of the HF TAC solutions.

The angular momentum of the considered system reads $\boldsymbol{I} = \mathcal{J}\boldsymbol{\omega} + \boldsymbol{s}$, where $\boldsymbol{s} = s_s \hat{\mathbf{1}}_s + s_l \hat{\mathbf{1}}_l$ is the vector sum of the spins of the gyroscopes. As in the cranking model, only uniform rotations ($\boldsymbol{\omega}$ constant in the body-fixed frame) will be considered. In this case, the Euler equations for rigid bodies [12] take the form $\boldsymbol{\omega} \times \boldsymbol{I} = 0$, thus requiring that $\boldsymbol{\omega}$ and $\boldsymbol{I}$ be parallel, like in self-consistent cranking solutions (Kerman-Onishi theorem [13]). These equations can easily be solved; a similar problem has been treated already in [14]. However, to show analogies with the HF method, here the variational principle will be employed. The Lagrangian of the system is equal to the sum of kinetic energies of the rotor and gyroscopes,

$$L = E_{\text{kin}} = \frac{1}{2}\boldsymbol{\omega}\mathcal{J}\boldsymbol{\omega} + \boldsymbol{\omega} \cdot \boldsymbol{s}; \tag{3}$$

the corresponding Hamiltonian $H = \boldsymbol{\omega} \cdot \boldsymbol{I} - L$. For the uniform rotation, $L$ is independent of time, hence the minimization of the action integral $\int L dt$ is equivalent to minimizing the Lagrangian as a function of the intrinsic-frame components of $\boldsymbol{\omega}$ for a fixed $\omega \equiv |\boldsymbol{\omega}|$. The solutions for uniform rotations can equally be obtained by finding extrema of the function $R = -L = H - \boldsymbol{\omega} \cdot \boldsymbol{I}$, which is the classical Routhian. Note that in the self-consistent cranking theory an analogous Routhian is minimized within the space of Slater determinants. Extrema of $R$ at a given $\omega$ can be found by using a Lagrange multiplier $\mu$ for $\omega^2$. Setting to zero the derivatives of the quantity

$$R + \frac{1}{2}\mu\omega^2 = \frac{1}{2}[(\mu - \mathcal{J}_s)\omega_s^2 + (\mu - \mathcal{J}_m)\omega_m^2 + (\mu - \mathcal{J}_l)\omega_l^2] - (\omega_s s_s + \omega_l s_l) \tag{4}$$

with respect to $\omega_m$, $\omega_s$, $\omega_l$, we obtain

$$\omega_m(\mu - \mathcal{J}_m) = 0, \tag{5a}$$

$$\omega_s = s_s/(\mu - \mathcal{J}_s), \tag{5b}$$

$$\omega_l = s_l/(\mu - \mathcal{J}_l). \tag{5c}$$

Equation (5a) gives either $\omega_m = 0$ or $\mu = \mathcal{J}_m$, leading to two distinct classes of solutions.

*Planar solutions.—If* $\omega_m = 0$, then both $\boldsymbol{\omega}$ and $\boldsymbol{I}$ lie in the *s-l* plane where also the spins of the gyroscopes are located. This gives planar solutions, for which the chiral

symmetry is conserved. All values of $\mu$ are allowed, and the Lagrange multiplier must be determined from given $\omega$. Figure 3(a) shows $\omega$ versus $\mu$ for sample model parameters extracted from the HF PAC calculations, see Table I. The solutions marked as $A$ and $D$ exist for all values of $\omega$. Above some threshold frequency, $\omega_{\rm thr}$, there appear two more solutions, ($B$, $C$). One finds easily

$$\omega_{\rm thr} = [(s_s)^{2/3} + (s_l)^{2/3}]^{3/2}/|J_l - J_s|. \qquad (6)$$

For the present case, $\omega_{\rm thr} > 1$ MeV/$\hbar$.

*Chiral solutions.—For* $\mu = J_m$, all values of $\omega_m$ are allowed, while the $\boldsymbol{\omega}$ components in the $s$-$l$ plane are fixed at $\omega_s = s_s/(J_m - J_s)$ and $\omega_l = s_l/(J_m - J_l)$. Consequently, the angular momentum has nonzero components along all three axes and the chiral symmetry is broken. For each value of $\omega$ there are two solutions differing by the sign of $\omega_m$, and thus giving the chiral doublet. Note that for $\omega_m = 0$ the chiral solution coincides with the planar $A$ band. The fact that $\omega_s$ and $\omega_l$ solutions are constant leads to the principal conclusion that chiral solutions cannot exist for $\omega$ smaller than the critical frequency

$$\omega_{\rm crit}^{\rm class} = \left[\left(\frac{s_s}{J_m - J_s}\right)^2 + \left(\frac{s_l}{J_m - J_l}\right)^2\right]^{1/2}. \qquad (7)$$

Its values for the parameters $J_{s,m,l}$ and $s_{s,l}$ extracted from the HF PAC calculations are listed in Table I.

Figure 3(b) presents the energy vs spin for the solutions to the classical model. At low spins, the yrast line coincides with the planar band $D$. Then it continues along the planar band $A$. Since the moment of inertia $J_m$ is the largest, beyond the critical frequency the chiral band becomes yrast, thereby yielding good prospects for experimental observation. These results agree with the HF TAC solutions, see Fig. 5.

Coming to the actual TAC calculations, by applying rotational frequency with nonzero $s$ and $l$ components, a HF planar band corresponding to the classical solution $A$ was obtained. At zero frequency, the angular momentum is just $\boldsymbol{s} = s_s\hat{\mathbf{1}}_s + s_l\hat{\mathbf{1}}_l$. Since $s_s$ and $s_l$ are almost equal, the initial tilt angle (between $\boldsymbol{\omega}$ and the long axis) is very close to 45°. With increasing $\omega$, the angular frequency vector tilts more and more towards the long axis, because $J_l > J_s$. This HF evolution of $\boldsymbol{\omega}$ is well reproduced by the classical model, see Fig. 4.

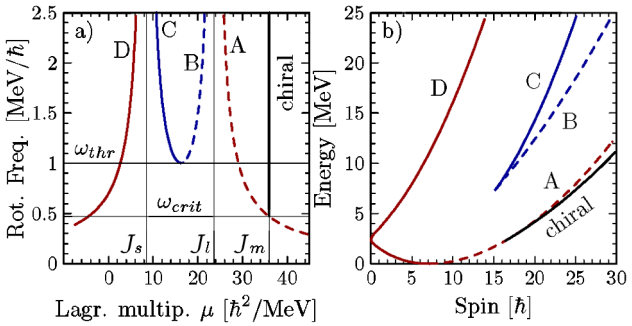


FIG. 3 (color online). (a) Rotational frequency $\omega = \omega(\mu)$ and, (b) Energy $E = E(I)$ for the four planar bands (marked $A$, $B$, $C$, $D$) and the chiral doublet (lines marked "chiral") obtained in the classical model. The model parameters, $J_{s,m,l}$ and $s_{s,l}$, are extracted from HF PAC calculations with the SLy4 force (see Table I).

In order to obtain the chiral solutions, to each converged point of the planar band a cranking frequency with nonzero $m$ component was applied. Chiral rotation appeared above some finite frequency $\omega_{\rm crit}^{\rm HF}$, given in Table I, while points of the planar band were obtained for lower frequencies. This confirms the existence of the critical frequency within the Skyrme-HF method. The evolution of $\boldsymbol{\omega}$ along the HF chiral band is shown in Fig. 4. There is again a qualitative agreement with the classical result and indeed, for $\omega = \omega_{\rm crit}^{\rm HF}$, the HF chiral and planar solutions coincide. Together with the critical frequencies, Table I lists the corresponding critical spins $I_{\rm crit}^{\rm class}$ and $I_{\rm crit}^{\rm HF}$. The HF results are not much, but systematically higher than the classical estimates.

The pure HF method does not take into account the pair correlations (superfluidity). To examine their possible role, PAC calculations within the total routhian surface (TRS) approach [15] were performed, with a phenomenological mean field and pairing in the usual pairing–self-consistent form. Deformation of $\beta \approx 0.20$ and $\gamma \approx 25°$ was obtained. TRS effectively interchanges the values of $J_s$ and $J_l$, and enlarges $J_m$ roughly twice with respect to the HF results. Qualitatively, these changes in the moments of inertia can be understood as consequences of the change in triaxiality $\gamma$. It is clear from Eq. (7) that an increase in $J_m$ may significantly lower the values of $\omega_{\rm crit}^{\rm class}$ and $I_{\rm crit}^{\rm class}$, see Table I. However, including pairing in the full HF TAC calculations (Hartree-Fock-Bogolyubov method) will be necessary to give more complete description.

The critical frequency represents the transition point between planar and chiral rotation. This transition is abrupt in the semiclassical cranking model, but rather

TABLE I. Moments of inertia $J_{s,m,l}$ [$\hbar^2$/MeV] and initial alignments $s_{s,l}$ [$\hbar$] obtained from HF and TRS PAC calculations together with the resulting values of the critical frequency and spin, $\omega_{\rm crit}^{\rm class}$ [MeV/$\hbar$] and $I_{\rm crit}^{\rm class}$ [$\hbar$], estimated from the classical model. Corresponding results from the full HF TAC calculations, $\omega_{\rm crit}^{\rm HF}$ and $I_{\rm crit}^{\rm HF}$, are also given.

| $J_s$ | $J_m$ | $J_l$ | $s_s$ | $s_l$ | $\omega_{\rm crit}^{\rm class}$ | $I_{\rm crit}^{\rm class}$ | $\omega_{\rm crit}^{\rm HF}$ | $I_{\rm crit}^{HF}$ |
|---|---|---|---|---|---|---|---|---|
| SLy4 | | | | | | | | |
| 8.45 | 36.0 | 23.7 | 5.60 | 5.21 | 0.47 | 16.4 | 0.60 | 20.3 |
| SKM* | | | | | | | | |
| 8.81 | 35.9 | 23.5 | 5.60 | 5.06 | 0.46 | 15.9 | 0.54 | 17.8 |
| TRS | | | | | | | | |
| 15.7 | 65.6 | 9.33 | 6.33 | 4.23 | 0.15 | 9.2 | | |

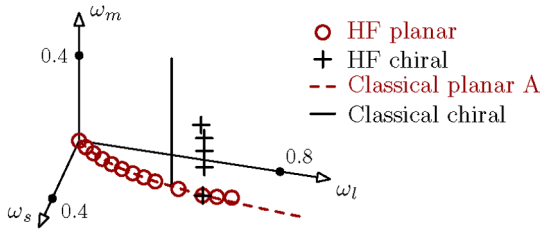


FIG. 4 (color online). Trajectory of the angular frequency vector in the intrinsic frame along the HF planar and chiral bands obtained with the SLy4 force, compared to the classical predictions. Scales are given in MeV/$\hbar$.

smooth in the fully quantum case. This is because the angular momentum vector oscillates about the planar equilibrium below $\omega_{\rm crit}$ (corresponding to nonuniform classical rotations [16]), and it can still tunnel between the left and right chiral minima above $\omega_{\rm crit}$ (chiral vibrations [2]). Since the mean-field approach does not take into account the interaction between the two minima, the HF chiral doublets are exactly degenerate. Therefore, the experimental splitting between the chiral partners cannot be calculated, and one can directly compare with experiment only the average trends and the value of the critical frequency or spin.

For some time, a closely lying side band in $^{132}$La has been interpreted as the chiral partner of the yrast band [5,17], but recently a third neighboring band was discovered [18], see Fig. 5. Whichever of them is the actual chiral partner, they are both located just below the HF TAC values of $I_{\rm crit}^{\rm HF}$, and just above the classical estimate $I_{\rm crit}^{\rm class}$ evaluated for the TRS PAC case. Their closeness to the possible values of $I_{\rm crit}$ suggests that they may represent a transition between planar and chiral rotation. At low spins, where the two candidate partners are not seen, the yrast band is well reproduced by the HF planar solution, see Fig. 5; at higher spins the correspondence is rather semiquantitative.

In summary, planar and chiral TAC solutions were found for the first time within a fully self-consistent microscopic approach and it has been shown that static chiral rotation can only take place above some finite angular frequency $\omega_{\rm crit}$. Basic features of the HF TAC bands can be understood in terms of a classical model that also gives an analytical estimate for $\omega_{\rm crit}$. From the present HF calculations without pairing, the value of $\omega_{\rm crit}$ is rather high as compared to the experimental candidate chiral bands in $^{132}$La. It seems that pairing can lower this value, and that the observed bands actually lie in the transitional region between planar and chiral rotation. Apart from taking into account pairing, further research may employ techniques beyond the mean field, which will allow to calculate the chiral splitting in the microscopic way.

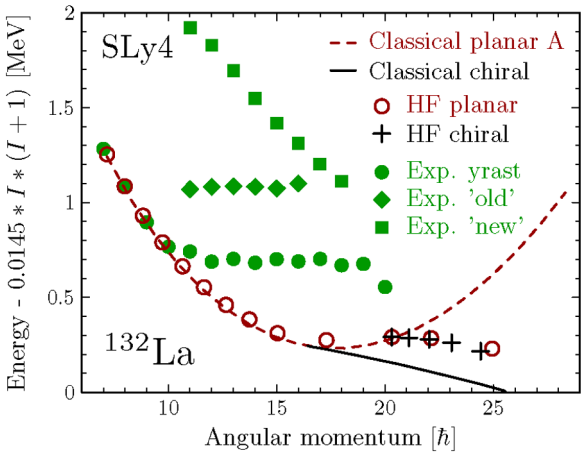


FIG. 5 (color online). Energies from the HF TAC and from the classical model, compared to the experimental data in $^{132}$La. The band marked "old" is the previously known candidate chiral partner [5]; the one marked "new" is the newly discovered third band [18]. (All bands are of the same parity.)

Comments by W. Nazarewicz, W. Satuła, K. Starosta, and Ch. Droste and co-workers are acknowledged. This work was supported in part by the Polish Committee for Scientific Research under Contract No. 5 P03B 014 21 and by the French-Polish integrated actions program POLONIUM.

[1] S. Frauendorf, Rev. Mod. Phys. **73**, 463 (2001).
[2] K. Starosta *et al.*, Phys. Rev. Lett. **86**, 971 (2001).
[3] S. Frauendorf and J. Meng, Nucl. Phys. **A617**, 131 (1997).
[4] A. Bohr and B. R. Mottelson, *Nuclear Structure* (Benjamin, New York, 1975), Vol. II.
[5] K. Starosta *et al.*, Phys. Rev. C **65**, 044328 (2002).
[6] S. Frauendorf, Nucl. Phys. **A557**, 259c (1993).
[7] V. I. Dimitrov, S. Frauendorf, and F. Dönau, Phys. Rev. Lett. **84**, 5732 (2000).
[8] E. Chabanat *et al.*, Nucl. Phys. **A627**, 710 (1997).
[9] J. Bartel *et al.*, Nucl. Phys. **A386**, 79 (1982).
[10] J. Dobaczewski and J. Dudek, Comput. Phys. Commun. **102**, 166 (1997); **102**, 183 (1997); **131**, 164 (2000).
[11] J. Dobaczewski and P. Olbratowski, Comput. Phys. Commun. **158**, 158 (2004).
[12] H. Goldstein, *Classical Mechanics* (Addison-Wesley, Cambridge, 1953).
[13] A. K. Kerman and N. Onishi, Nucl. Phys. **A361**, 179 (1981).
[14] A. M. Kamchatnov, J. Phys. G **16**, 1203 (1990).
[15] W. Satuła and R. Wyss, Phys. Rev. C **50**, 2888 (1994).
[16] V. Dimitrov, F. Dönau, and S. Frauendorf, nucl-th/0211063.
[17] J. Timár *et al.*, Eur. J. Phys. A **16**, 1 (2003).
[18] E. Grodner *et al.*, Int. J. Mod. Phys. E **13**, 243 (2004).